On Atomic Line Opacities for Modeling Astrophysical Radiative Transfer

Jonathan Morag*

¹Weizmann Institute of Science, Rehovot, Israel

23 September 2025

ABSTRACT

In astrophysics, line opacity is a primary source of uncertainty in theoretical calculations of radiative transfer. Much of this uncertainty is dominated by the inability to resolve the width and separation in frequency of sharp atomic transition lines, leading to the common use of approximate frequency-averaged treatments for the lines. In a previous paper, we calculated shock-cooling emission following explosions in core-collapse supernovae using a mult-group radiative transfer code, and compared the results to those of the similar and often used STELLA code from the literature. We found important differences in the spectral energy distribution (SED) resulting from different choices of line opacity treatment. In our code, we used in the emissivity a frequency-binned average of a high-resolution opacity, while in STELLA the often-used Eastman Pinto 1993 (EP93) prescription was employed. In this short letter we revisit this comparison, essentially reproducing STELLA's bound-free (photoionization) and bound-bound (line transition) opacities. We show the importance of introducing micro-plasma electron excitation level cutoffs in the equation of state (EOS). We also argue that EP93 is useful for estimating photon mean free-path in the presence of a forest of lines, but that it can underestimate photon production and reprocessing rates (emissivity) by orders of magnitude. To our knowledge, no fully-consistent coarse-frequency solution currently exists for line modeling in these systems.

Finally, we describe new features in our updated publicly available high-resolution frequency-dependent opacity table.

Key words: radiation: dynamics – supernovae: general

1 INTRODUCTION

Calculating radiative transfer in high-energy astrophysical contexts often requires input of the photon to plasma interaction cross-section ("opacity"), which introduces considerable theoretical uncertainty. A primary challenge involves the implementation of sharp atomic transition lines, whose widths and separations in wavelength can be many orders of magnitude smaller than the resolution currently available in simulation, and whose strengths can be orders of magnitude above the scattering opacity. Due to these and additional challenges (e.g. incomplete corresponding laboratory measurements, common uncontrolled assumptions such as plasma local thermal equillibrium, and complex plasma microsphysics), a fully self-consistent calculation of the "bound-bound" line interaction is not currently available.

In expanding supersonic flows, the presence of a thick forest of lines can significantly reduce the propagating photon's mean-free-path as it Doppler shifts in frequency. This effect is often included in line treatments that derive a coarse frequency-averaged approximation of the opacity for use in radiative transfer (Karp et al. 1977; Friend & Castor 1983; Eastman & Pinto 1993; Blinnikov 1997). These "expansion opacity" formalisms are based on similar assumptions (see § 3) and have been shown to be in general agreement with each other (Castor 2007; Potashov et al. 2021), especially in the limits of all-weak or all-strong lines.

Of these methods, the formalism of Eastman & Pinto (1993, hereafter EP93) has been commonly used in the community (e.g. Blinnikov et al. 1998; Tominaga et al. 2011; Förster et al. 2018; Ben Nasr et al. 2023; Gallego et al. 2024), including in Monte-Carlo simulations (Kasen et al. 2006; Kawaguchi et al. 2020; Barnes et al. 2021; Domoto et al. 2022; Bulla 2023)².

In a previous paper, Morag et al. (2024, hereafter M24), we solved numerically for the observed shock cooling emission from optically thick, ionized ejecta in core-collapse supernovae. We compared our spectral energy density (SED) results to several works in the literature that were produced using the STELLA code (Blinnikov et al. 1998; Tominaga et al. 2011; Kozyreva et al. 2020a). Our code and STELLA are similar. Both codes employ a 1-dimensional radiative transfer 'multi-group' treatment, where the photons are binned into frequency groups and radiative transfer for each bin is solved separately. Bound-bound opacity in both cases is solved using experimentally verified atomic line lists by Kurucz (1995). Though the two sets of results appear to be in agreement regarding hydrodynamics and energy budget, there is a marked difference in the output spectrum (orders of magnitude in some frequency bands) primarily due to our

to be in reasonable agreement with Eastman & Pinto (1993), at least relative to the orders of magnitude disagreements we report in this letter.

^{*} E-mail: jmorag88@gmail.com

¹ Blinnikov (1997) actually provides a mono-chromatic description for the bound-bound opacity, and has been shown, after coarse frequency averaging,

² Monte-Carlo methods have an intuitive advantage for line forests but face a similar challenge in resolution for describing the emissivity. Other approaches to the problem include using steady-state methods, low optical depths and/or fully incorporating at least a subset of the involved atomic lines without use of the expansion formalism (Lucy 2002, 2003; Kromer & Sim 2009).

different respective choices of line treatment leading to varying levels of reprocessing.

In this short letter we dive further into the comparison in an attempt to better account for the differences in line treatment in coarse-frequency grids for optically thick supersonic flows. We focus here on reproduction of the STELLA opacities given in Blinnikov et al. (1998, hereafter B98). We use this comparison to assess the validity of the commonly employed Eastman & Pinto (1993, hereafter EP93) prescription. The paper is written as follows. We reproduce the B98 photo-ionization "bound-free" opacity in § 2, and bound-bound opacity in § 3. In § 4 we discuss and summarize, and also announce useful updates to our publicly available-frequency dependent opacity table, given in M23.

2 BOUND-FREE OPACITY AND EQUATION OF STATE (EOS)

Computing the equation of state (EOS) requires the use of a limiting physical cutoff for the allowed excited bound electron states due to micro-interactions between nearby species in the plasma. Without such a cutoff, the atomic partition function diverges. In our opacity table we address this effect in Hydrogen by adopting a prescription from Hummer & Mihalas (1988), which forbids highly excited states due to the presence of nearby ions in the plasma. We use these states to solve the Saha equation self-consistently assuming LTE.

In fig. 1 we compare only bound-free opacity κ_{ν} from B98 fig. 1 at top (here in black line) to that produced by our table (M23 - blue line). There is an orders of magnitude difference between the two tables for Hydrogen photoionization peaks ($\lambda > 500$ Å). Since the photoionization for Hydrogen is given by simple analytic relations, and since the He cross-sections ($\lambda \leq 500$ Å) are in reasonable agreement for the two formulations, the difference between the opacities is very likely a result of different implementations of the H equation of state. Specifically, there is a likely difference in the ionization level and the population of electrons at each excited atomic level.

We are able to reproduce the B98 opacity to a factor of a few when we don't implement the Hummer Mihalas factor in Hydrogen, and when we arbitrarily cut off the number of Hydrogen levels to $n_{\rm max} = 400$ (in this case, Hummer Mihalas should greatly restrict the presence of electrons above $n \sim 10's - 100$). As EOS calculations tend to be complex, the exact reason for the discrepancy is unknown to us, and we do not know which implementation is more correct. We note however, that in M24, we showed that the M23 table agrees with the publicly available TOPS table (Colgan et al. 2016) with regards to the bound-free opacity to $\sim 10\%$.

The presence of the strong Hydrogen photo-ionization cross-section in Blinnikov et al. (1998) likely accounts for the sharp photo-ionization cutoff observed in the SED in Tominaga et al. (2011), which uses STELLA. Due to our much lower bound-free opacity, and different implementation of atomic transition lines (see below) we do not observe such a cutoff when using our M23 table (see M24).

We also note that the introduction of the Hummer Mihalas factor can either increase κ_{ν} or decrease it, depending on implementation and whether or not it is employed in the Saha equation to decide ionization, or in the bound-free and bound-bound opacities to determine the bound electron excitation populations. In general, some excitation level cutoff and test of convergence should be included in both.

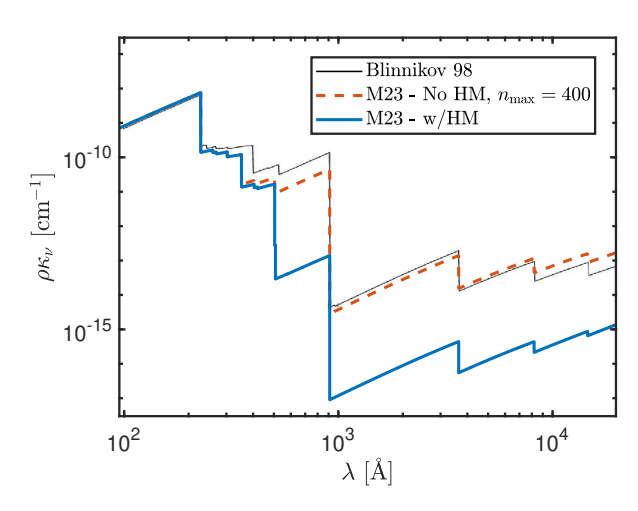


Figure 1. Our imitation of the bound-free opacity in B98 (black line) for the example case of $\rho = 10^{-13}~{\rm cm}^{-3}$, $T = 15,000~{\rm K}$ for a solar mixture. In red dashed-line, we show the result when the Hummer & Mihalas (1988) factor is not included, and we limit the Hydrogen partition function to $n_{\rm max} = 400$, finding reasonable agreement with B98. In blue solid lines we show the result of a converged H partition function, representative of what we insert into the simulations in M24. The difference in the opacities can be orders of magnitude in the H photoinization opacity (He photoinization is less affected).

3 BOUND-BOUND OPACITY

In fig. 2 we reproduce an example bound-bound opacity from B98 fig. 1 (center) that is used in STELLA, sampled in a grid of $(\Delta\nu/\nu)_i\sim 0.01$. The i subscript denotes a binned frequency group. We find good agreement to a factor of a few. Normally, emission and absorption opacities from our high frequency resolution M23 opacity table are calculated using a frequency average across each bin, $\langle\kappa_{\nu}\rangle_i$. In this reproduction, we used the same excitation and ionization electron populations from our original code and (EOS), but averaged line strengths according to the approximate Eastman & Pinto (1993) prescription that is used in STELLA. EP93 describes the mean free-path of a photon in a line forest as it Doppler shifts in frequency in the expanding flow. It is given by

$$\chi_{\exp,i} = \rho \kappa_{\exp,i} = (\nu/\Delta \nu)_i (ct_{\exp})^{-1} \sum_{I} [1 - \exp(-\tau_I)], \tag{1}$$

where the sum l is performed over all lines within the frequency bin i $(\nu, \nu + \Delta \nu)$ containing many lines. The line Sobolev optical depth τ_l is given by

$$\tau_l = c t_{\rm exp} [1 - \exp(-h\nu_l/T)] \sigma_l n_{e,jl} / \nu_l, \quad \sigma_l = \pi \left(e^2/m_{\rm e}c\right) f_l.$$
 (2)

Here m_e is the electron mass, v_l and f_l are the line frequency and oscillator strength, $n_{e,l}$ is the bound-electron number density in the excited state corresponding to the lower energy level of the atomic transition line. The expansion time $t_{\rm exp}$ is a placeholder for the local velocity shear $\sim (dv/dr)^{-1} \sim (v/r)^{-1}$, equivalent everywhere to a single value (the dynamical time t) in the case of homologous expansion.

In fig. 3 we show the same comparison but now at a lower frequency resolution ($[\Delta \nu/\nu]_i \sim 0.1$), similarly to B98 fig. 1 at bottom. Here we zoom out and add a comparison to our 'static' opacity (not incorporating Doppler expansion) at the same density and temperature. We show both the frequency bin averaged $\langle \kappa_{\nu} \rangle_i$ and the bin Rosseland mean $\kappa_{R,i}$. Our static κ_R , which is used to determine radiative transfer (diffusion) in M24, is insensitive to the presence of

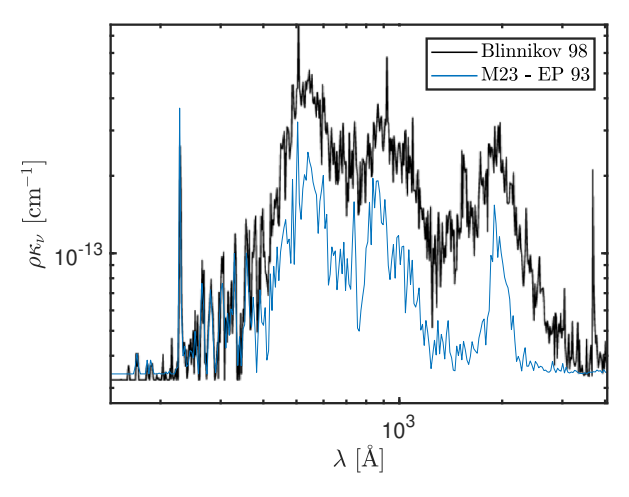


Figure 2. Bound-bound opacity example from B98 fig. 1, compared with our reproduction using M23 modified to employ the EP93 prescription. We finding good agreement to a factor of a few or better. The plasma parameters are $\rho = 10^{-13}~{\rm cm}^{-3}$, $T = 15,000~{\rm K}$, $t_{\rm exp} = 15$ days. Similarly to B98, we use a coarse frequency grid with $\Delta v/v \sim 0.01$. The lines that are in excellent agreement in the range 200 Å < λ < 400 Å are dominated by a Helium line ($\lambda = 227 {\rm \AA}$) and a set of Oxygen lines.

lines. It does not exhibit large deviations from the electron scattering opacity $\kappa_{\rm es}$, and is similar in this case to EP93 (not including bound-free opacity - see fig. 3 caption). On the other hand, $\langle \kappa_{\nu} \rangle_{\rm i}$, which is used in M24 in the emission / absorption term, is higher than the EP93 result by orders of magnitude. We also show in fig. 3 that in the early limit, $t_{\rm exp} \to 0$, the expansion opacity approaches $\langle \kappa_{\nu} \rangle_{\rm i}$. The behavior in this limit can be deduced analytically from eqs. 1 and 2.

As $t_{\rm exp}$ increases, the rate of photon frequency shift due to velocity shear decreases. Therefore, τ_l increases linearly with time as photons passing through the line spend longer in resonance. Meanwhile, photons also spend longer traveling in between lines, hence the $(ct_{\rm exp})^{-1}$ factor in eq. 1. Since the contribution of each strong line is counted as at most $[1-\exp(-\tau_l)] \to 1$, the net effect is a reduction of the opacity over time as more lines become stronger and saturate (i.e. $\kappa_{\rm abs} \to 0$ as $t_{\rm exp} \to \infty$). For the (ρ,T) parameter choice in this example, the EP93 opacity is already lower from the static result by up to an order of magnitude when $t_{\rm exp} = 1$ hr. Consequently the effect of lines when using EP93 during shock-cooling is very weak.

4 SUMMARY AND DISCUSSION

In this letter we showed that the choice of line treatment in simulation can have an orders of magnitude effect on the introduced opacity, focusing on non-relativistic optically thick plasma. In § 2 and fig. 1, we compared the *bound-free* opacity from our opacity table in Morag (2023, - M23), against the opacity given in the literature by Blinnikov et al. (1998, - B98), finding orders of magnitude difference. We concluded that the discrepancy in the tables in bound-free processes is likely due to deviations in the underlying plasma equation of state (EOS). We previously showed in Morag et al. (2024, - M24) that our bound-free opacity agrees with TOPS (Colgan et al. 2016), another opacity table from the literature. In § 3 (figs. 2 and 3) we made a similar comparison, focusing on *bound-bound* opacity. We were able to reproduce the opacities presented in B98 by employing the EP93 prescription (eqs. 1 and 2). At the expansion time $t_{\rm exp}$ presented, this reproduced opacity was found to be orders

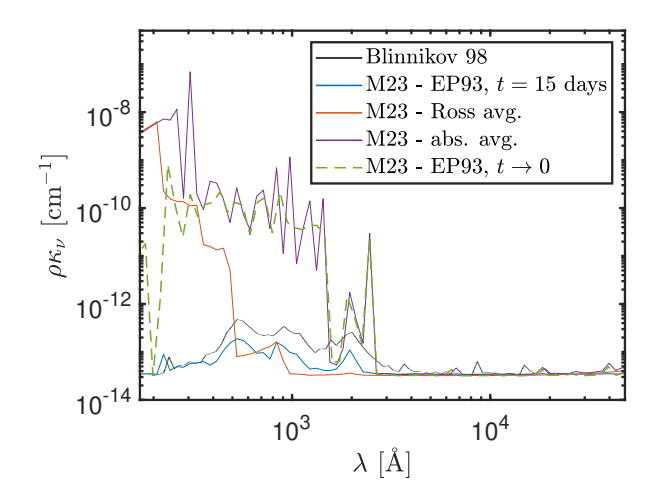


Figure 3. Same as fig. 3, at lower frequency resolution $(\Delta v/v \sim 0.1)$. For ease of comparison, the $\kappa_{\rm es}$ baseline has been added to the average and EP 93 opacities, despite not normally being added to the emission / absorption terms. The Ross mean opacity also includes bound-free opacities (unlike other opacities in the figure), as these cannot be separated in a harmonic average.

of magnitude lower than the 'static' average absorption opacity $\langle \kappa_{\nu} \rangle_{i}$ extracted from the high-resolution M23 table.

The different opacity results can lead to important differences in the calculated SED (see the example of shock cooling emission in M24). If the approximate static $\langle \kappa_{\nu} \rangle_i$ is used to calculate emissivity in radiative transfer calculations, the presence of a line forest at energies $h\nu \gtrsim 3T$ can lead at peak energy frequencies to considerable reprocessing, even out to low scattering optical depths (τ < 1). The resulting SED at these frequencies would then appear similar to a blackbody at the local temperature (if the plasma itself is near LTE). The effect of photoionization peaks in this case would generally be negligible. On the other hand, if the EP93 approximation is used instead, photons formed inside at many scattering optical depths $(\tau \sim 100$'s-1000's) can undergo only limited reprocessing. The peak photon energy would be representative of the temperatures at these depths, leading to a shift of the peak relative to a blackbody. In this case the sharp effect of photoionization opacity can become more observable as well.

The EP93 prescription is useful in the context of radiative transfer for calculating the photon mean-free-path, as the photon shifts in frequency across transition lines. For a particular frequency group, it is then reasonable in optically thick supersonic flows to calculate the scattering opacity as (see also Mihalas & Mihalas 1999; Castor 2007)

$$\kappa_{\text{scat},i} \to \max(\kappa_{\text{R},i}, \kappa_{\text{EP93},i}).$$
(3)

This approach also addresses a shortcoming of the Sobolev approximation that EP93 is based on, as Sobolev does not include line wings, which can have a significant effect on the continuum (provided the wings are included in calculating κ_R).

EP93 is less useful for calculating the photon emission and absorption rates (emissivity) $c\rho\kappa_{\nu}$, as it ignores the maximum line strength (recall that the contribution from each line is capped at $(\nu/\Delta\nu)_i(ct_{\rm exp})^{-1}\times 1$). The correct total photon production rate should be given by $\langle\kappa_{\nu}\rangle_i$ independent of velocity shear. This approach however is also not ideal, as the photons in a coarse multi-group calculation are assumed to be produced uniformly in frequency across a group, which is not the case physically. A correct description of the

photon *absorption* is even more complex, as it depends on the local photon energy distribution u_{ν} , which can be uneven at line frequency resolutions.

It is possible that the true spectrum results lie somewhere in between the two prescriptions. Though EP93 is likely an underestimate of the emissivity, it is also possible to overestimate the emission / absorption processes when using the average absorption opacity (see M24 for details). We note however, that in the thermalized limit of strong absorption, there is weak sensitivity to the exact absorption amount. This insensitivity occurs since additional absorption, regardless of the details, only helps to further maintain thermal equilibrium. We also previously verified the M24 results that used $\langle \kappa_{\nu} \rangle_i$ for shock-cooling emission by showing agreement with a separate post-processing calculation. This high frequency resolution calculation resolved individual lines and included the effect of expansion opacity, providing a separate measure of validity.

In the above discussion we assumed that all lines are absorptive as opposed to representing scattering events (Baron et al. 1996; Blinnikov et al. 1998; Hillier & Dessart 2012; Kozyreva et al. 2020b). This would imply high bound electron relaxation rates relative to the photo-transition rates. This is something that should be verified per use case (see for example M24). However, it is possible that the effect of relaxation may be calculated more accurately by including the relaxation rate into the numerics. Several works address this head-on by relaxing the assumption of LTE in the plasma and calculating specific rates for competing atomic processes, albeit for a subset of the species (e.g. Lucy 2002, 2003; Kromer & Sim 2021; Pinto & Eastman 2000; Dessart et al. 2015). For other works that assume local thermal equilibrium of the plasma (LTE), we suggest that the frequency-dependent emission/absorption opacity may be modified as

$$\kappa_{\nu, \text{abs}} \to \min(\kappa_{\nu, \text{abs}}, R/\rho c),$$
(4)

where the relaxation rate $R = \text{func}(l, v, \rho, T, \text{composition})$ can be estimated analytically -with some care- and this can be done prior to inserting into the numerics in most schemes. In this suggested scheme, atomic transitions that emit and absorb faster than the relaxation rate will reprocess at most at the relaxation rate, and will behave as scattering events above this rate. Using this scheme would reduce the need for an uncertain parameter describing whether line interactions represent absorption or scattering events, as is often done in the literature (e.g. Blinnikov et al. 1998; Kozyreva et al. 2020b; Morag et al. 2024).

An updated version of our frequency-dependent opacity table is now available in Morag (2023). The calculations for producing a high resolution table are the same as described in the previous version in M24. However, we add additional features for use in analysis and simulation. These include functions that provide opacity κ_R and $\langle \kappa_{\nu} \rangle_i$ averages for coarse frequency resolution MG simulations. The update includes approximations for the EP93 expansion opacity, including (eqs. 1 and 2) for MG simulations. It also allows for direct broadening and shifting of the high-resolution table for arbitrary choices of v/c.

REFERENCES

Barnes J., Zhu Y. L., Lund K. A., Sprouse T. M., Vassh N., McLaughlin G. C.,
Mumpower M. R., Surman R., 2021, The Astrophysical Journal, 918, 44
Baron E., Hauschildt P. H., Nugent P., Branch D., 1996,
Monthly Notices of the Royal Astronomical Society, 283, 297

Ben Nasr S., Carvajal Gallego H., Deprince J., Palmeri P., Quinet P., 2023, Astronomy & Astrophysics, 678, A67

Blinnikov S. I., 1997, in Ruiz-Lapuente P., Canal R., Isern J., eds,

NATO ASI Series, Thermonuclear Supernovae. Springer Netherlands, Dordrecht, pp 589–605, doi:10.1007/978-94-011-5710-0_36, https://doi.org/10.1007/978-94-011-5710-0_36

Blinnikov S. I., Eastman R., Bartunov O. S., Popolitov V. A., Woosley S. E., 1998, The Astrophysical Journal, 496, 454

Bulla M., 2023, Monthly Notices of the Royal Astronomical Society, 520, 2558

Castor J. I., 2007, Radiation Hydrodynamics. Cambridge, UK; New York Colgan J., et al., 2016, The Astrophysical Journal, 817, 116

Dessart L., Audit E., Hillier D. J., 2015, Monthly Notices of the Royal Astronomical Society, 449, 4304

Domoto N., Tanaka M., Kato D., Kawaguchi K., Hotokezaka K., Wanajo S., 2022, The Astrophysical Journal, 939, 8

Eastman R. G., Pinto P. A., 1993, The Astrophysical Journal, 412, 731

Friend D. B., Castor J. I., 1983, The Astrophysical Journal, 272, 259

Förster F., et al., 2018, Nature Astronomy, 2, 808

Gallego H. C., Pain J.-C., Godefroid M., Palmeri P., Quinet P., 2024, Journal of Physics B: Atomic, Molecular and Optical Physics, 57, 035001

Hillier D. J., Dessart L., 2012, Monthly Notices of the Royal Astronomical Society, 424, 252

Hummer D. G., Mihalas D., 1988, The Astrophysical Journal, 331, 794
Karp A. H., Lasher G., Chan K. L., Salpeter E. E., 1977, The Astrophysical Journal, 214, 161

Kasen D., Thomas R. C., Nugent P., 2006, The Astrophysical Journal, 651,

Kawaguchi K., Shibata M., Tanaka M., 2020, The Astrophysical Journal, 889,

Kozyreva A., Nakar E., Waldman R., Blinnikov S., Baklanov P., 2020a, Monthly Notices of the Royal Astronomical Society, 494, 3927

Kozyreva A., Shingles L., Mironov A., Baklanov P., Blinnikov S., 2020b,
 Monthly Notices of the Royal Astronomical Society, 499, 4312

Kromer M., Sim S. A., 2009, Monthly Notices of the Royal Astronomical Society,

Kromer M., Sim S. A., 2021, Astrophysics Source Code Library, p. ascl:2103.020

Kurucz R. L., 1995, in ASP Conference Series. p. 583, http://adsabs.harvard.edu/abs/1995ASPC...81..583K

Lucy L. B., 2002, Astronomy and Astrophysics, 384, 725

Lucy L. B., 2003, Astronomy and Astrophysics, 403, 261

Mihalas D., Mihalas B. W., 1999, Foundations of Radiation Hydrodynamics. Mineola, NY

Morag J., 2023, Frequency Dependent Opacity Table, https://github.com/jon-morag/Freq_Dept_Opac_Table/

Morag J., Irani I., Sapir N., Waxman E., 2024, Monthly Notices of the Royal Astronomical Society, 528, 7137

Pinto P. A., Eastman R. G., 2000, The Astrophysical Journal, 530, 757

Potashov M. S., Blinnikov S. I., Sorokina E. I., 2021, Astronomy Letters, 47, 204

Tominaga N., Morokuma T., Blinnikov S. I., Baklanov P., Sorokina E. I., Nomoto K., 2011, The Astrophysical Journal Supplement Series, 193, 20

APPENDIX A: COMMENTS ON USING THE OPACITY TABLE

We add here a few suggestions regarding the use of the Morag (2023) opacity table.

Our code implements the Hummer & Mihalas (1988) microplasma suppression factor, which is given as a function of quantum number n for H-like ions only. For mixtures that are not dominated by H, the user may choose to implement an approximate extension for non-H-like ions. Under the approximation that a sufficiently excited single electron sees a screened H-like ion, its effective H-like quantum number is then given by

$$n_{\text{eff}} = Z_{i} \sqrt{I_{R}/(I_{i} - E_{s})}. \tag{A1}$$

Here Z_i is the net screened nuclear charge number the excited electron sees, $I_R = 13.6$ eV, $I_i > 0$ is the ionization energy of the particular ionization state, and $E_s > 0$ is the energy of the state measured from the ionization ground state. This prescription suppresses multiple excited electron states (perhaps unnaturally) due to their higher energy.

Several functions exist in the M23 code for checking convergence of the opacity table with respect to the total number of states in the partition function. These functions artificially either remove or extend the number of included excited electron states.

Finally, we remind the user that when producing our simulations in M24, we artificially removed a handful of extremely strong lines that appeared, as these led to an overestimate of the flux. We suggests for users to consider doing the same when producing simulations.

This paper has been typeset from a TEX/LATEX file prepared by the author.